HOSTED BY

ELSEVIER

Available online at www.sciencedirect.com

ScienceDirect

Journal of Magnesium and Alloys 4 (2016) 68–76
www.elsevier.com/journals/journal-of-magnesium-and-alloys/2213-9567

Full Length Article

Influence of bimodal grain size distribution on the corrosion behavior of friction stir processed biodegradable AZ31 magnesium alloy

N. Saikrishna [a], G. Pradeep Kumar Reddy [b], Balakrishnan Munirathinam [c], B. Ratna Sunil [a,*]

[a] Department of Mechanical Engineering, Rajiv Gandhi University of Knowledge Technologies (AP-IIIT), Nuzvid 521202, India
[b] Department of Mechanical Engineering, Vignana Bharathi Institute of Technology, Hyderabad 501301, India
[c] Department of Metallurgical and Materials Engineering, Indian Institute of Technology Madras, Chennai 600036, India

Received 28 September 2015; revised 26 December 2015; accepted 31 December 2015

Available online 26 February 2016

Abstract

In the present study, AZ31 magnesium alloy sheets were processed by friction stir processing (FSP) to investigate the effect of the grain refinement and grain size distribution on the corrosion behavior. Grain refinement from a starting size of 16.4 ± 6.8 μm to 3.2 ± 1.2 μm was attained after FSP. Remarkably, bimodal grain size distribution was observed in the nugget zone with a combination of coarse (11.62 ± 8.4 μm) and fine grains (3.2 ± 1.2 μm). Due to the grain refinement, a slight improvement in the hardness was found in the nugget zone of FSPed AZ31. The bimodal grain size distribution in the stir zone showed pronounced influence on the corrosion rate of FSPed AZ31 as observed from the immersion and electrochemical tests. From the X-ray diffraction analysis, more amount of $Mg(OH)_2$ was observed on FSPed AZ31 compared with the unprocessed AZ31. Polarization measurements demonstrated the higher corrosion current density for FSPed AZ31 (8.92×10^{-5}A/cm^2) compared with the unprocessed condition (2.90×10^{-5}A/cm^2) that can be attributed to the texture effect and large variations in the grain size which led to non-uniform galvanic intensities

Keywords: AZ31 Mg alloy; Biodegradable implants; Grain size distribution; Corrosion; Friction stir processing, texture

1. Introduction

Magnesium (Mg) and its alloys are now gaining immense importance as promising candidates for load bearing temporary implant applications in biomedical engineering. Biocompatibility, biodegradability and mechanical properties close to that of natural human bone are the advantages with the magnesium [1]. Avoiding the necessity of second surgical procedure to remove the implant after the tissue is healed and reducing the other complications such as restenosis, thrombosis, permanent physical irritation, and inability to adapt to growth and changes in human body are the major benefits with the magnesium based temporary implants [1,2]. However, the high corrosion rate of magnesium in the biological environment is the major concern in developing magnesium based implants which also influences the healing rate [3,4]. Therefore, different strategies such as developing new alloys, composites and coatings have been widely adopted to address the uncontrolled degradation issue of magnesium [4–13]. Microstructural modification is another interesting route recently gaining wide popularity to alter the corrosion rate of magnesium [14–22].

AZ series (Aluminum and zinc) is the well-known Mg alloy system commonly used in the structural applications [23]. Mg alloy with 3% Al and 1% Zn (AZ31) is one of the most widely investigated compositions among the other AZ series Mg alloys for biomedical applications because of less aluminum content. If aluminum content is increased more than 3%, the presence of more $Mg_{17}Al_{12}$ phase at the grain boundaries significantly influences the mechanical and corrosion properties of Mg alloys [24]. Additionally, good fatigue and corrosion resistance also made AZ31 Mg alloy as first choice for medical implant applications [20].

It is an interesting observation in the literature that the grain refinement has increased the corrosion resistance [14–22] and also as reported in some studies, decreased the corrosion resistance [20–22,25] of Mg alloys. Usually the grain boundaries are

* Corresponding author. Department of Mechanical Engineering, Rajiv Gandhi University of Knowledge Technologies (AP-IIIT), Nuzvid 521202, India. Tel.: +91 9677119819; fax: +08656 235150.

E-mail addresses: bratnasunil@gmail.com, bratnasunil@rgukt.in (B. Ratna Sunil).

http://dx.doi.org/10.1016/j.jma.2015.12.004
2213-9567/

the high energy sites so that the corrosion is initiated preferentially from the grain boundaries. Fine grain structure increases the fraction of grain boundary and hence reduces the corrosion resistance of the material in the aggressive medium. However, ability to quickly form a protective passive layer helps to reduce the corrosion rate of fine grained metals in the neutral electrolyte and such behavior can be found in metals like Mg alloys. Therefore, microstructural modification can be adopted as a promising method in corrosion management of reactive metals like Mg alloys. In addition to this, the level of secondary (β) phase distribution in the alloy or some dissolved elements in the alpha phase (solid solution) also improve the corrosion resistance.

Severe plastic deformation (SPD) techniques are the recently emerged potential top-down methods used to achieve grain refinement in metals [26]. Friction stir processing (FSP) is one of such methods in which the microstructure of metallic sheets or plates can be modified by using a non-consumable rotating tool consisting a shoulder and pin. The mechanism behind grain refinement during FSP has been explained elsewhere [27]. There are a few reports clearly demonstrating the improved corrosion resistance of Mg alloys after FSP [15–18,28]. A few studies have also clearly shown the abnormal change in the electrochemical behavior due to texture [29–32]. However, the information regarding the electrochemical behavior of Mg alloys which exhibit varying levels of grain refinement (bimodal grain size) is lacking. It has been well understood that FSP does not always yield uniform grain refinement which depends on various process parameters [27]. Therefore, in the current study, AZ31 Mg alloy was selected and was processed by FSP to modify the microstructure. Corrosion studies were carried out by the immersion test and electrochemical method with an aim to understand the corrosion behavior of AZ31 Mg alloy with bimodal grain size distribution. The effect of distributed grain size on hardness was also measured and discussed.

2. Materials and methods

2.1. Experimental details

AZ31 Mg alloy rolled sheets (Exclusive Magnesium, Hyderabad) of chemical composition 2.75% Al, 0.91% Zn, 0.001% Fe, 0.01% Mn and remaining being Mg were cut into 100×100×4 mm^3 size and annealed at 340 °C for 1 h. Friction stir processing (FSP) was carried out using an automated universal milling machine (Bharat Fritz Werner Ltd., India). FSP tool made of H13 tool steel was used to process the samples. FSP tool has a shoulder of diameter 20 mm and a tapered pin with root diameter of 3 mm, end diameter of 1 mm and a length of 3 mm. Initially, trial experiments were conducted to optimize the process parameters to get defect free stir zone. Then the FSP was carried out with a tool travel speed of 100 mm/min at a tool rotational speed of 1100 rpm. The penetration depth (3 mm) was given such a way that the tool shoulder touches the work piece surface. The processed AZ31 was coded as FSPed AZ31.

2.2. Material characterization

Specimens of 30 mm length were cut across the FSPed zone and metallographic polishing was done using different graded emery papers. The specimens were then polished using diamond paste of 3 μm size using a disc polishing machine. After each step, the samples were cleaned in distilled water, wiped with cotton and soaked in ethanol to remove any water remaining on their surface. Picric acid reagent comprised of 5 g picric acid, 5 ml acetic acid, 5 ml distilled water and 100 ml ethanol was prepared as etching agent. The polished samples were etched in the solution for 20 seconds and then cleaned in distilled water followed by cleaning in ethanol. The microstructural observations were carried out using an optical microscope (Leica, Germany) at different areas of interest on the surface and cross sections of FSPed regions. Average grain size was measured by linear intercept method.

2.3. Microhardness

Microhardness measurements (Omnitech, India) were carried out on polished specimens by applying 100 g load with 10 sec dwell period. One measurement was obtained for each 1 mm distance. The indents were placed across the FSPed regions at the surface and cross sections. Microhardness was measured over a distance across the stir zone such a way that the base material hardness was also measured up to 5 mm away from the stir zone.

2.4. Corrosion studies

2.4.1. Immersion test

Immersion studies were carried out in 0.9% NaCl solution for 1, 2 and 3 days to assess the corrosion rate of the samples. Lab grade NaCl (Merc, India) was used to prepare 0.9% NaCl solution using de-ionized water and the samples of size $10 \times 10 \times 1.5$ mm^3 were immersed in the solution and the containers were kept at 37 °C in a constant temperature water bath. The ratio of the volume of the solution to the surface area of the specimens was kept more than 1:10. Weights of all these samples before and after immersion were measured. For each group (Unprocessed and FSPed), three samples were considered (n = 3) and immersion studies were carried out. The samples were taken from the solution after each day and gently rinsed in stable de-ionized water and dried. The samples were then immersed in boiling solution of chromic acid (180 g/one liter of de-ionized water) to remove the surface corrosion products. Then the samples were dried in air before measuring the weight loss. Corrosion rate was calculated according to ASTM standard NACE TM0169/ G31 – 12a as given below [33].

$$\text{Corrosion rate}\,(\text{mm/year}) = k \times \Delta W/(A \times T \times D) \quad (1)$$

where $k = 8.76 \times 10^4$, T = time of exposure in hours, A = area of the specimen in cm^2, ΔW = weight loss in g, D = density in g/cm^3.

2.4.2. Electrochemical test

Electrochemical studies were carried out using 0.9% NaCl solution as the electrolyte using Gill AC potentiostat (ACM

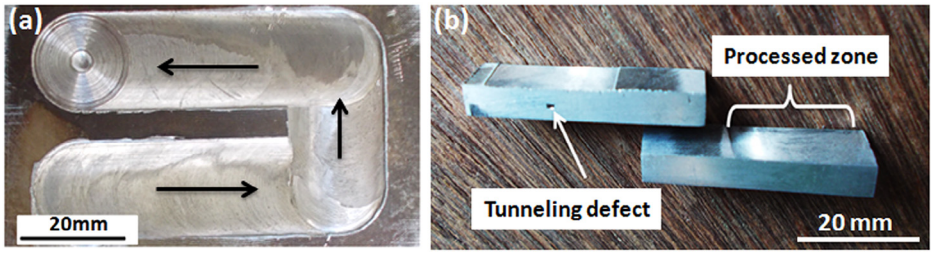

Fig. 1. Photograph of FSPed AZ31 sample: (a) processed region and (b) cut samples showing cross section with defect (during process parameters optimization) and without defect (after processing with optimized parameters).

Instruments, UK). During the measurements, graphite rod was used as a counter electrode and a saturated calomel electrode (SCE) as a reference electrode with the specimen (area 1 cm^2) as working electrode. All potentials in the paper were measured with reference to SCE. Potentiodynamic polarization was recorded at a scan rate of 1 mVs^{-1} after stabilizing the system to the open circuit condition for 1 hour. Corrosion current density (i_{corr}) and corrosion potential (E_{corr}) were obtained from the polarization plots using Tafel extrapolation method [34]. The corrosion rate (CR) was calculated using the following equation [34].

$$\mathrm{CR\,(mils/year)} = 0.129 \times a \times i_{corr} / n\,D \quad (2)$$

where CR is the corrosion rate, a is the Molar mass (for magnesium 24.3 g/mol), i_{corr} is the corrosion current density in $\mu A/cm^2$, n is the valance and D is the density (1.74 gm/cm^3). The obtained CR was converted into mm/year by considering 1 mils/year equal to 0.0254 mm/year.

2.5. Characterization after immersion test

Scanning electron microscopy (SEM, FEI Quanta 200, Netherlands) was carried out to observe the surface morphologies of the samples after immersion studies. Energy dispersive X-ray spectroscopy (EDS) was done to observe the elemental composition of the corrosion products. The samples before and after the immersion test were analyzed by X-ray diffraction (XRD) method (D8 Advanced, Bruker, USA) with Cu Kα radiation (λ = 1.54 Å) at a scanning rate of 1 step/s and step size of 0.15°/step.

2.6. Statistical analysis

Statistical analysis was done by one way ANOVA method (using Origin Pro 8, USA). $P < 0.05$ was considered as statistically significant.

3. Results

3.1. Microstructural observations

A photograph of friction stir processed (FSPed) AZ31 sheet is shown in Fig. 1(a). Black arrows indicate the stirring direction. Fig. 1(b) shows the photograph of the through hole (known as tunneling defect) appeared to be parallel to the direction of FSP at the cross section and also defect free stir zone after FSP with optimized parameters. Fig. 2 shows the optical micrographs of unprocessed AZ31 (coded as AZ31) and FSPed AZ31 obtained at the cross section. It is clear from the observations that the nugget zone has not completely refined but presence of large grains was noticed. The magnified images (Fig. 2(b) and (c)) clearly show that the grain refinement was happened in two different scales. Combination of coarse grains and fine grains in the nugget zone resulted in mixed microstructural features. The level of grain refinement was found to be more at the regions where the material has undergone severe plastic deformation. Therefore, dynamic recrystallization was initiated and fine grains were evolved during FSP.

Fig. 3 compares the microstructure of AZ31 before and after FSP. From a starting grain size of 16.4 ± 6.8 μm, grain refinement was observed and measured as 3.2 ± 1.2 μm after FSP. However, there are a few regions of coarse grains within the nugget zone similar to the starting grain size which is a clear indication of grain growth due to the heat generated during the process. Due to the generated heat beneath the nugget zone, the grain size was found to be increased when compared with the starting size as shown in Fig. 3(c). A few interesting microstructural features were observed within the nugget zone as shown in Fig. 4. Alternate regions of fine and coarse grains in a stacked pattern appeared within the nugget zone which is usually called as onion ring patterns in FSPed samples. These patterns directly indicate the complex nature of material plastic flow and different levels of grain refinement during FSP.

3.2. Microhardness

The microhardness distribution as shown in Fig. 5 depicts the dependence of hardness on grain size. As most of the FSPed zone has grain size distribution over a long range, the microhardness values also showed a significant variation (Fig. 5(a)). But it can be observed that the hardness over the surface of FSPed AZ31 was slightly increased compared with AZ31. There is also a significant difference in the microhardness of AZ31 and FSPed AZ31 (both across the stir zone surface and cross section) as shown in Fig. 5(b). Higher average hardness values at the surface and lower average hardness values at the cross section of FSPed AZ31 were observed when compared with AZ31.

3.3. Corrosion studies

Fig. 6 shows the photographs of the samples before and after immersion studies (after the corrosion products were removed).

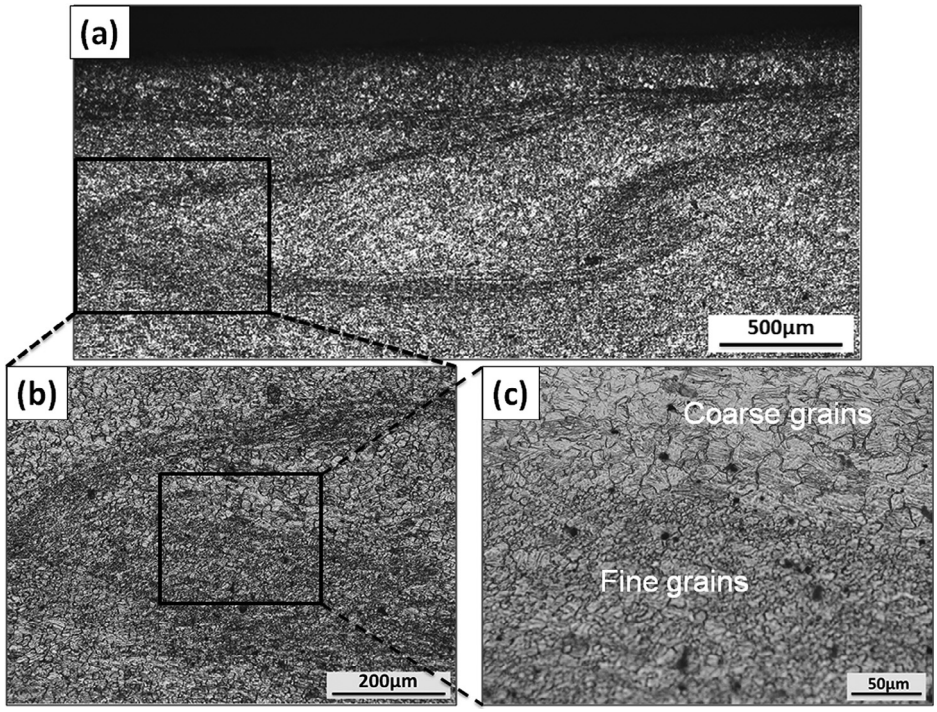

Fig. 2. Optical micrographs of nugget zone (a) image showing material flow in low magnification, (b) magnified image showing presence of fine and coarse grains and (c) high magnified image showing a clear difference in grain size at the nugget zone.

It can be seen that all the samples have undergone localized corrosion. Fig. 7(a) shows weight loss measurements for the samples after 1, 2 and 3 days. The weight loss for AZ31 followed a systematic increment with the increase in immersion time. But, for FSPed AZ31, the weight loss did not follow any particular trend indicating abnormal behavior. Fig. 7(b) shows potentiodynamic polarization curves of the samples. FSPed AZ31 showed higher corrosion current densities compared with

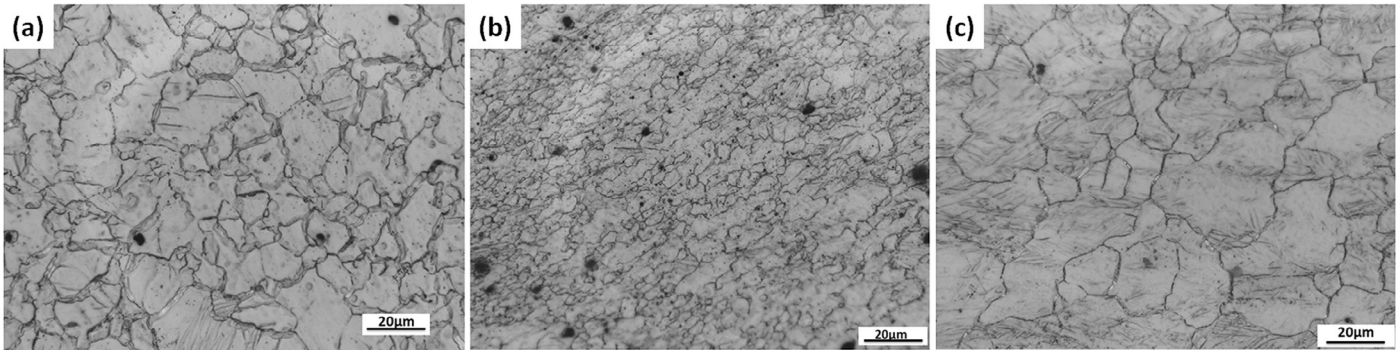

Fig. 3. Optical micrographs: (a) AZ31, (b) FSPed AZ31 (in the nugget zone) and (c) bottom of the nugget zone.

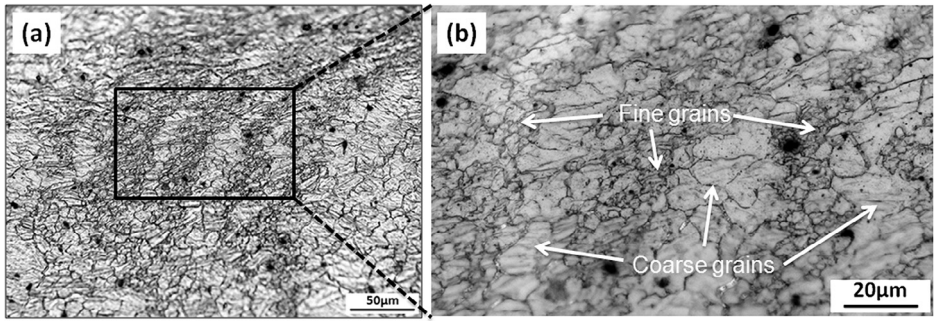

Fig. 4. Optical micrographs showing material flow patterns in the nugget zone.

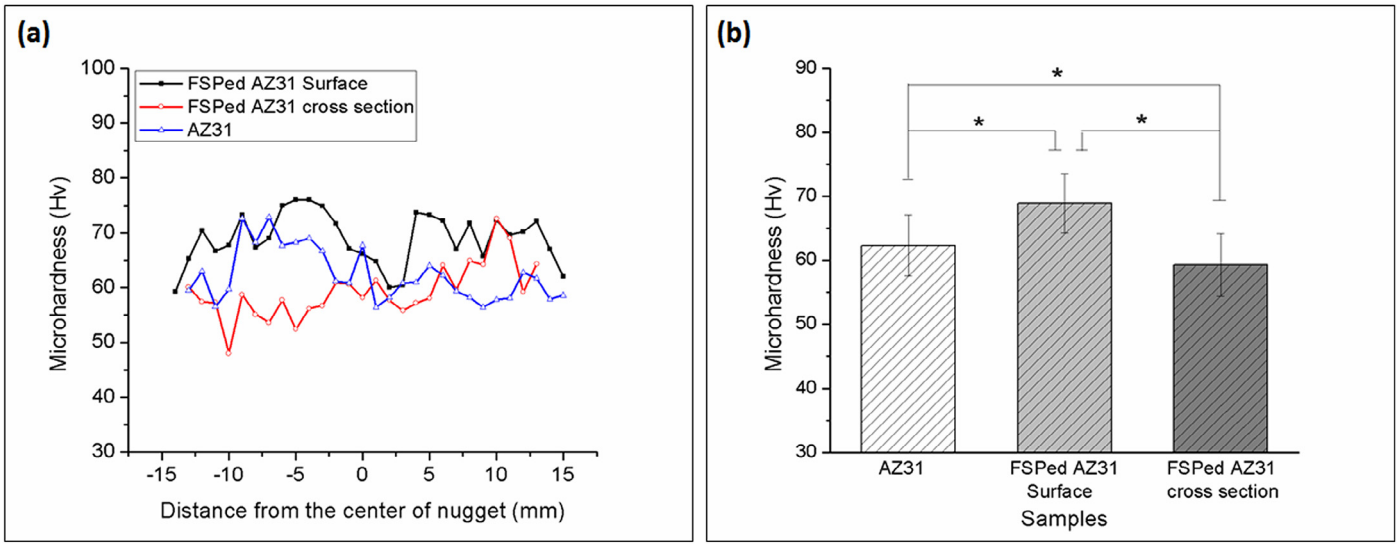

Fig. 5. Microhardness measurements: (a) hardness distribution and (b) average hardness measured across the surface and the cross section (* statistical analysis was done by one way ANOVA method and $p < 0.05$ has been considered as statistically significant).

AZ31. The corrosion potentials showed noble behavior for AZ31 compared with FSPed AZ31. The electrochemical results were in agreement with immersion test results. The results from both the immersion and electrochemical studies demonstrated a slight decrease in corrosion resistance of FSPed AZ31. Table 1 lists the electrochemical parameters of the samples obtained from potentiodynamic polarization tests. Table 2 compares the corrosion rates of the samples obtained from both the immersion and electrochemical tests. The corrosion rates of the samples were found to be decreased as the immersion time was increased to 3 days. Decrease in the corrosion rate was more for FSPed AZ31 (from 9.9 to 4.63 mm/year) compared with AZ31 (from 6.04 to 3.99 mm/year) as the immersion time was increased from 24 h to 72 h. There is a clear difference between the corrosion rate calculated from immersion studies and electrochemical studies. However, similar behavior can be noticed

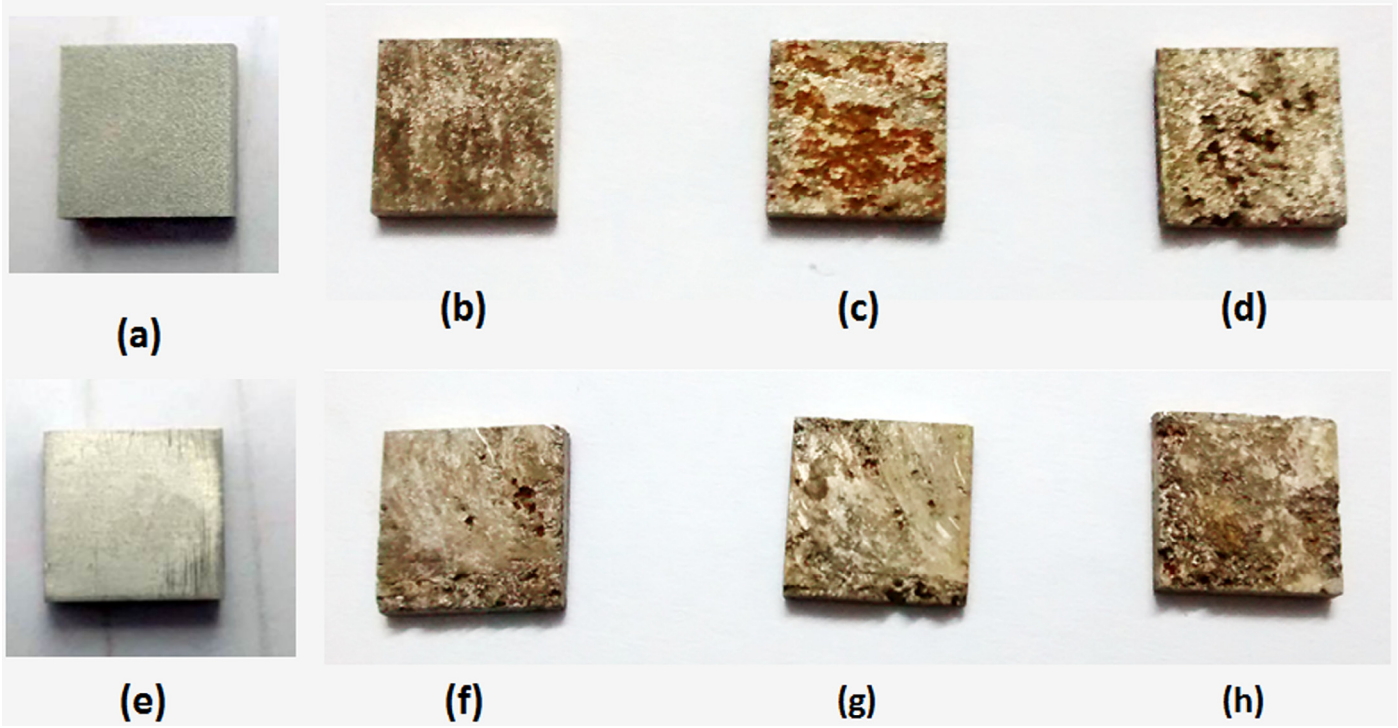

Fig. 6. Typical photographs of the samples (of size $10 \times 10 \times 1.5$ mm^3) before and after immersion test: (a) AZ31 before immersion, (b) AZ31 after 24 h of immersion, (c) AZ31 after 48 h of immersion, (d) AZ31 after 72 h of immersion, (e) FSPed AZ31 before immersion, (f) FSPed AZ31 after 24 h of immersion, (g) FSPed AZ31 after 48 h of immersion and (h) FSPed AZ31 after 72 h of immersion.

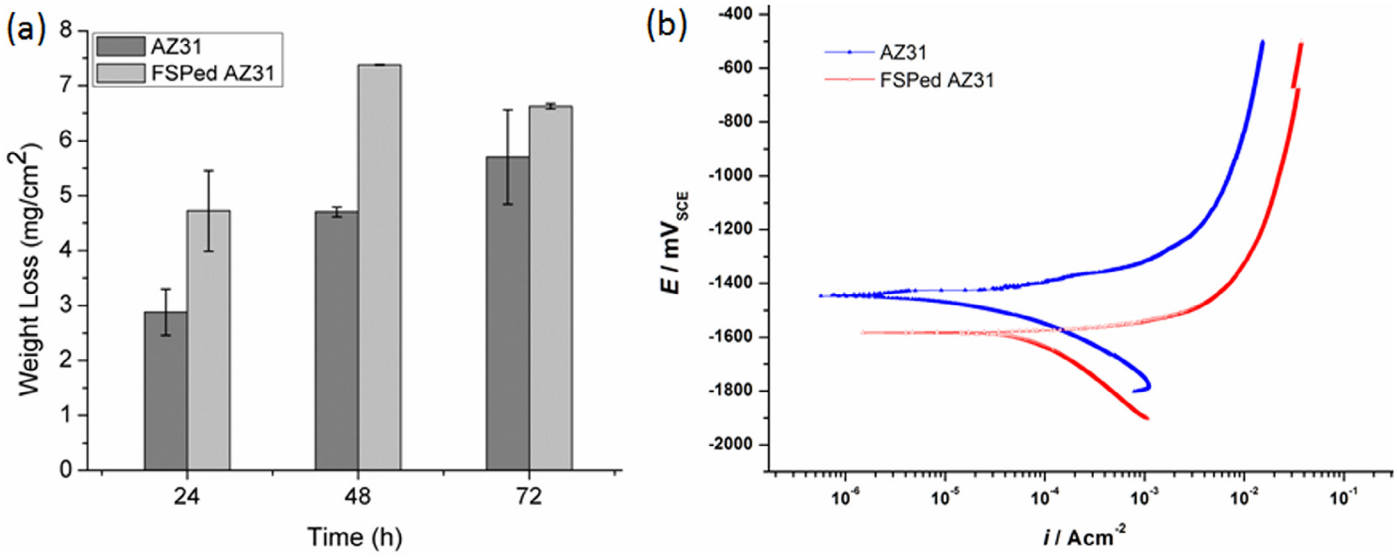

Fig. 7. Corrosion studies of the samples: (a) weight loss obtained from immersion test and (b) potentiodynamic polarization curves of the samples in 0.9% NaCl solution.

in both the cases where FSPed AZ31 exhibited more corrosion rate compared with AZ31.

Fig. 8 shows SEM micrographs of the samples after 3 days of immersion in 0.9% NaCl solution. During the 1st and 2nd days, the entire sample surfaces were observed as degraded with large cracks and pits. As immersion time was increased to 3 days, FSPed AZ31 surface was found to be more degraded compared with that of AZ31. From the EDS analysis (Fig. 8(c) and (f)), presence of magnesium, oxygen, aluminum and chlorine was clearly observed at the surface of the immersed samples. The presence of Cl was not noticed after 1 and 2 days of immersion from the EDS studies but found to increase as the immersion time is increased to 3 days.

The presence of Cl suggests the formation of magnesium chloride as the solution has chloride ions abundantly. Presence of magnesium and aluminum elements in the EDS analysis is obvious from the base material composition. Magnesium forms magnesium hydroxide ($Mg(OH)_2$) in any aqueous solutions and therefore the presence of oxygen in the present study can be attributed to the formation of $Mg(OH)_2$. This was also confirmed by XRD (Fig. 9) analysis. Peaks (001), (101), (102), (110) and (111) corresponding to $Mg(OH)_2$ were identified and indexed in the XRD patterns. From the 1st day of immersion, all the samples have shown the presence of $Mg(OH)_2$ layer. The normalized intensities of (001) and (101) peaks corresponding to $Mg(OH)_2$ were observed as prominent compared with AZ31 samples for all the 3 days. The results suggest the presence of more amount of $Mg(OH)_2$ on FSPed AZ31 samples compared with AZ31 sample. The normalized intensities of (100) and (101) peaks were found to be increased and the intensity of (002) plane was reduced for FSPed AZ31 compared with that of AZ31 which suggest the orientation change of the grains within the nugget zone. Indeed, the texture in a polycrystalline metal influences the surface properties as the number of atoms available in close packed planes is more compared with the other planes.

Table 1
Electrochemical parameters of the samples obtained from potentiodynamic polarization tests.

Sample	i_{corr} (10^{-5}A/cm^2)	E_{corr} (mV$_{SCE}$)
AZ31	2.90	−1446.9
FSPed AZ31	8.92	−1583.1

Table 2
Comparison of corrosion rates of the samples obtained from immersion test and electrochemical test.

Test	Time (h)	Corrosion rate (mm/year)	
		AZ31	FSPed AZ31
Immersion test	24	6.04	9.90
	48	4.93	7.75
	72	3.99	4.63
Electrochemical test	–	0.47	2.04

4. Discussion

Grain size plays a predominant role in altering the material properties. In polycrystalline metals, grain boundary and grain interior exhibit different characteristics and hence the increased fraction of grain boundary influences structure sensitive properties such as yield strength, electrical conductivity, corrosion rate, etc. Along with the grain size, the other microstructural features such as stacking faults, dislocations, size and distribution of secondary (β) phase and also the type of grain boundary (twin, low angle or high angle) influence the bulk properties of a polycrystalline metal. Therefore, grain refinement may not always improve the properties but may introduce the contrary effects. In general, electrochemical events depend on various factors and may not happen similarly in all the metals which have the same grain size. Especially for Mg and its alloys, along

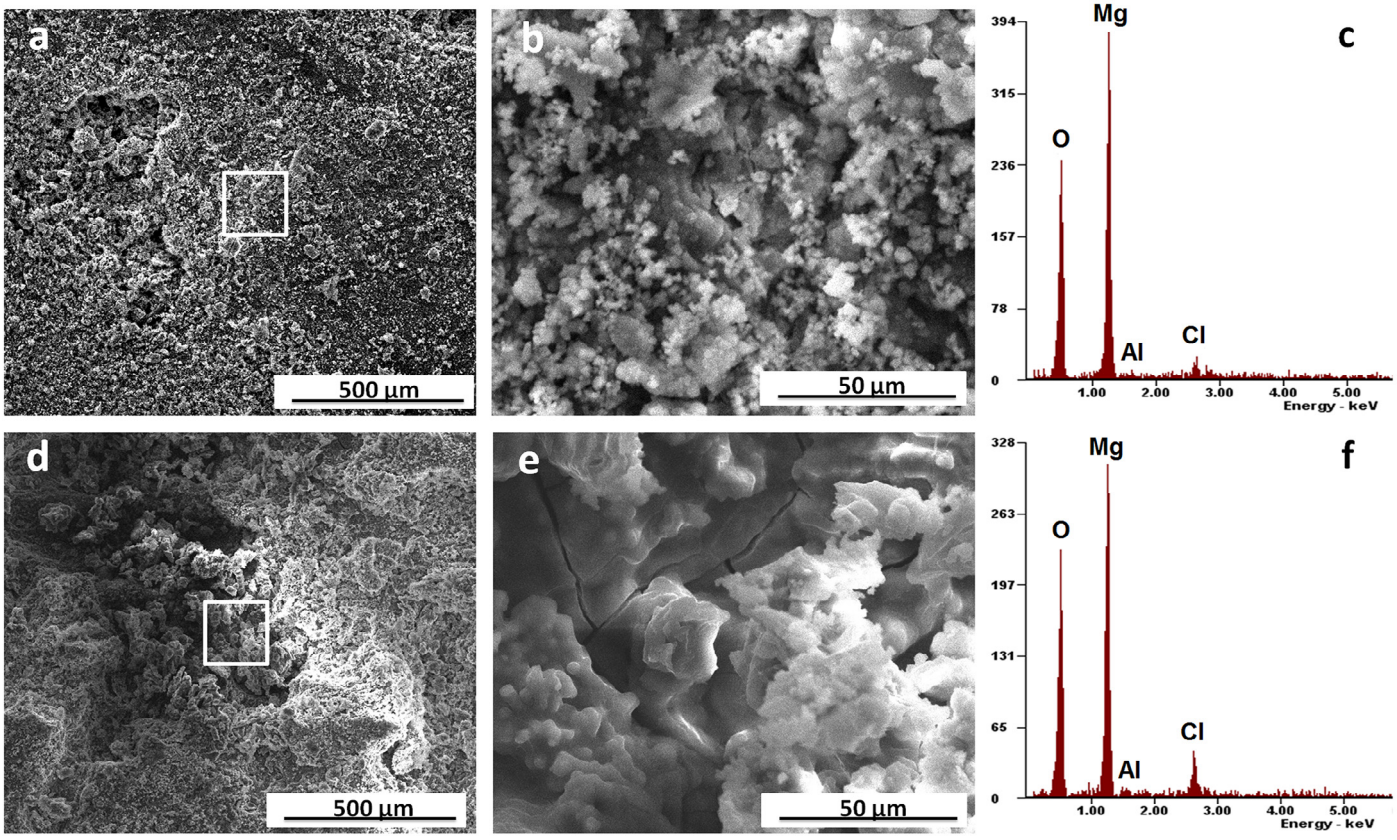

Fig. 8. SEM micrographs and EDS analysis of the phases present at the surface after 72 h of immersion in 0.9% NaCl solution.

with grain refinement, other factors which influence the corrosion rate must be considered to evaluate the corrosion performance. That is the valid reason to explain why there are a few reports which showed the increased corrosion resistance with grain refinement [14–22] and also decreased corrosion rate with grain refinement [20–22,25].

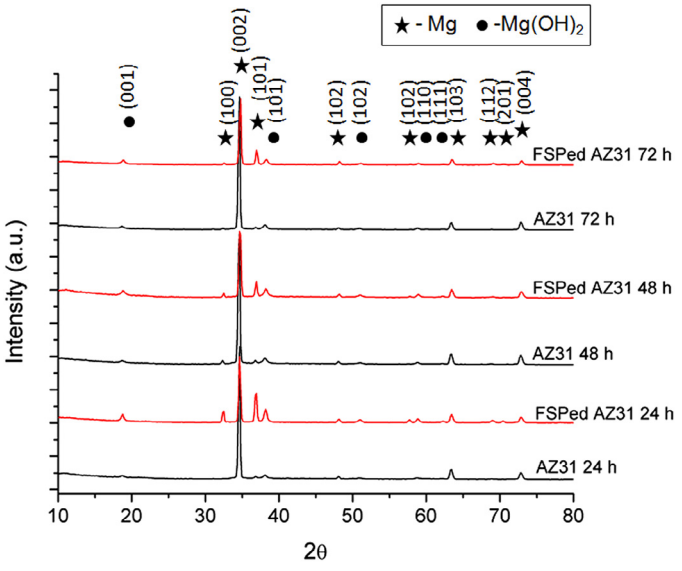

Fig. 9. XRD patterns of the samples after immersion study.

In the current work, there is a large distribution in the grain size within the nugget zone starting from 3.8 ± 1.2 µm to 11.6 ± 8.4 µm (Fig. 3). Compared with starting grain size 16.4 ± 6.8 µm, the nugget zone contained non-uniform grain size. In our earlier study, uniform grain size was observed (from a starting size of 56 µm to 4 µm after FSP) in FSPed AZ31 processed with similar processing parameters but with a different tool design [35]. The ratio of tool shoulder diameter (15 mm) to tapered pin base diameter was kept as 3 in the earlier work. Whereas in the present study, the ratio is 6.67 (shoulder diameter is 20 mm). As the tool shoulder diameter was increased, the heat generation at the stir zone also enormously increased due to the more frictional area at the tool and work piece interface compared with the previous studies. Therefore, the excess heat that has been produced during FSP led to grain growth and produced a combination of fine and coarse grains as shown in Fig. 2. As explained by Arbegast [36], material flow during FSP is complex in nature which includes different metal forming zones such as extrusion zone and forging zone along with preheat and post heat zones. The excessive material flow due to the localized extrusion at the vicinity of the FSP tool pin and also dynamic recrystallization during FSP led to evolve fine grains in the stir zone. Simultaneously, excess generation of heat caused the grain growth and therefore a combination of fine and coarse grains appeared in the stir zone as shown in Fig. 4.

The influence of non-uniform grain size has been clearly reflected in the microhardness measurements (Fig. 5). Usually, smaller grain size increases the hardness. Due to the presence of coarse grains within the stir zone, a large distribution in the hardness values can be seen as shown in Fig. 5(a). Nevertheless, a significant difference was observed in the average hardness before and after FSP. Interestingly, higher hardness at the surface and lower hardness at the cross section of FSPed AZ31 was noticed which suggests the grain growth as the reason behind the reduced hardness in the thickness direction as seen at the bottom of the stir zone (Fig. 3). More grain growth in the thickness direction can be attributed to the more heat concentration compared with the surface which promotes the evolution of large grains compared with starting grain size [37]. Heat loss by the conduction through the FSP tool and convection to the atmosphere reduces the total heat concentration at the surface compared with the stir zone in the thickness direction [38]. From the microhardness measurements, the decrease in the hardness was found to be marginal and which is less concerned since the mechanical properties of natural bone are even less than the properties of unprocessed pure Mg.

Interestingly, a considerable difference was noticed between the corrosion rates obtained by immersion test and electrochemical test. In electrochemical test, the work piece is subjected to polarization in order to record the corresponding current densities to assess its corrosion behavior. Whereas in immersion test, the work piece is exposed to corroding environment without subjecting to any potential changes. However, both methods can be used to relatively estimate the corrosion behavior of the samples. From both the corrosion tests, the corrosion resistance of FSPed AZ31 was observed to be reduced compared with AZ31. It is a clear observation from the potentiodynamic polarization curves that the anodic region of both the curves traces the similar path revealing the non-passive nature of the samples. Corrosion current density has no significant influence on the processing condition but AZ31 showed comparatively less i_{corr} value compared with FSPed AZ31. The anodic film is more likely to be formed on all samples, but the breakdown of this layer is inevitable in the presence of chloride ions as observed for FSPed AZ31 samples. E_{corr} value for FSPed AZ31 was decreased about 120 mV compared with AZ31 due to the increased anodic dissolution rates. $Mg(OH)_2$ is the corrosion product resulted when Mg is immersed in any aqueous solution due to the anodic and cathodic reactions [4]. This semi-protective layer protects the Mg and avoids further corrosion. But in the presence of chloride ions, $Mg(OH)_2$ is unstable and leads to form magnesium chloride which is an easily dissolvable salt [4,8]. More amount of Cl observed on FSPed AZ31 sample from EDS analysis after 72 h of immersion indicates the formation of more magnesium chloride which also confirms the increased corrosion rate after FSP. In order to decrease the uncontrolled degradation rate, the rate of magnesium chloride formation must be reduced. That can be achieved by providing elements which can readily form chlorides before magnesium chloride is formed and stabilize the passive layer. Another approach is providing a surface coating which reduce the attack of the aggressive chloride ions.

Basically, grain boundary and grain size are the two major influencing factors to get affected by microstructural modifications in mechanical processing. In Mg, grain boundary acts as cathode and grain interior acts as anode. Secondary (β) phase also acts as cathode and corrosion kinetics are severely affected. The role of β phase is negligible in AZ31 Mg alloy, but the role of grain size is predominant. Intensity of galvanic couple is reduced and also quick semi-protective anodic layer is formed if the grain size of Mg alloys is reduced as reported in the literature [17,18]. Bobby Kannan et al. [15] demonstrated a slight increase in the corrosion resistance for FSPed AZ31 Mg alloy and suggested that the β phase ($Mg_{17}Al_{12}$) dissolution due to FSP led to decrease the galvanic corrosion and enhanced the corrosion resistance after FSP. But, from their microstructural studies, the grain refinement was found to be insignificant and the grain size after FSP was uniform. Interestingly in the present study, the corrosion rate was surprisingly increased for the bimodal grain size. From the XRD studies (Fig. 9), the intensity of (002) peak was found to be reduced and the intensities of (100) and (101) peaks were found to be increased after FSP. Since the corrosion resistance is more for higher atomic density planes [39,40], FSPed AZ31 has shown increased corrosion rate as the intensity of the higher atomic density planes was reduced after FSP. Xin et al. [29,30] and Song [31] have also clearly demonstrated the effect of preferred orientation in enhancing the corrosion resistance of AZ31. Abnormal distribution of galvanic intensities, particularly at the grain boundary, might have raised the corrosion current density of FSPed AZ31. Therefore, it can be understood from the current study that the texture and grain size distribution are the two important mechanisms which have played prominent role compared with the dissolution of the β phase by FSP and reduced the corrosion resistance. From the present study, another influencing factor known as bimodal grain size was also found to be prominent in effecting the electrochemical behavior of AZ31. Hence, it is suggested that the uniform grain size is preferred compared with bimodal distribution in order to increase the corrosion resistance. However, concerning the mechanical properties, bimodal grain size may be helpful but uniform grain size is suggested for Mg based degradable implant applications where the degradation rate plays a crucial role. Therefore, if the targeted application is to function in any corroding environment containing lower or negligible amount of chloride ions, even bimodal grain size distribution can be suggested. But, if the intended application is for biodegradable implants where the surrounding environment contains higher amounts of chloride ions, bimodal distribution of grain size is not suggested. Therefore, it can be understood that the mechanical processing such as FSP can be adopted to reduce the grain size of AZ31 Mg alloy to utilize the advantage of grain refinement in developing Mg based degradable implants but obtaining uniform grain size is preferable compared with bimodal grain size distribution in order to reduce the corrosion rate. It is true that the actual biological system contains other ions, proteins, minerals and growth factors along with local tissue interactions. These bio-interactions also influence the corrosion of the implant. The effect of bimodal grain size distribution and the presence of

texture on these bio-reactions are not yet clearly understood. The role of bimodal grain size distribution on the mechanical performance of AZ31 Mg alloy when exposed to corroding environment or in physiological environment is also required to be explored.

5. Conclusions

In the present investigation, friction stir processing was chosen to alter the microstructure of AZ31 Mg alloy targeted for degradable implant applications and the following conclusions can be drawn:

1 Grain refinement was achieved by FSP from a starting size of 16.4 ± 6.8 μm to 3.2 ± 1.2 μm but due to the higher heat generation during processing, grain growth along with dynamic recrystallization produced a large variation in the grain size (3.8 ± 1.2 - 11.6 ± 8.4 μm).
2 Bimodal grain size distribution was found to have a significant effect on the microhardness as reflected in the variations in the hardness measurements observed within the stir zone. There was a significant deference between the surface and cross section hardness which is due to the difference in microstructure evolution in thickness direction.
3 Corrosion studies confirmed the increased corrosion rate for FSPed AZ31 (0.445 mm/year) compared with AZ31 (0.134 mm/year) which can be mainly attributed to the texture and bimodal grain size distribution.
4 It has been clearly understood that the grain size distribution also plays a crucial role along with the texture and grain size in corrosion management of Mg alloys in developing degradable implants which further needed to be investigated in detail.

Acknowledgements

The authors would like to thank Dr. Lakshman Neelakantan, Department of MME, IIT Madras, for helping in corrosion studies. Thanks are due to Mr. V. Sunil Raj, Lab assistant, Department of MME, RGUKT, Nuzvid for helping in characterization of the samples.

References

[1] F. Witte, N. Hort, C. Vogt, S. Cohen, K.U. Kainer, R. Willumeit, et al., Curr. Opin. Solid State Mater. Sci. 12 (2008) 63–72.
[2] B.A. Shaw, E. Sikora, S. Virtanen, Fix, Heal, and Disappear: A New Approach to Using Metals in the Human Body, The Electrochemical Society Interface – summer 45–49, 2008.
[3] K. Sigrid, J.G. Brunner, F. Ben, V. Sannakaisa, J. Biomed. Mater. Res. Part B Appl. Biomater. 96B (2011) 84–90.
[4] R. Zeng, W. Dietzel, Adv. Eng. Mater. 10 (8) (2008) B3–B14.
[5] F. Witte, V. Kaese, H. Haferkamp, E. Switzerc, A. Meyer-Lindenberg, C.J. Wirth, et al., Biomaterials 26 (2005) 3557–3563.
[6] H. Hornberger, S. Virtanen, A.R. Boccaccini, Acta Biomater. 8 (2012) 2442–2455.
[7] S. Shaylin, J.D. George, Acta Biomater. 8 (2012) 20–30.
[8] H. Wang, Y. Estrin, Z. Zúberová, Mater. Lett. 62 (2008) 2476–2479.
[9] X.B. Chen, N. Birbilis, T.B. Abbott, Corrosion 67 (3) (2011) 035005-1–035005-16.
[10] A. Zakiyuddin, K. Lee, J. Alloys Compd. 629 (2015) 274–283.
[11] B. Ratna Sunil, T.S. Sampath Kumar, U. Chakkingal, V. Nandakumar, M. Doble, Mater. Sci. Eng. C Mater. Biol. Appl. 39 (2014) 315–324.
[12] G. Keerthi Soujanya, T. Hanas, V. Yogeshwar Chakrapani, B. Ratna Sunil, T.S. Sampath Kumar, Procedia Mater. Sci. 5 (2014) 817–823.
[13] B. Ratna Sunil, C. Ganapathy, T.S. Sampath Kumar, J. Mech. Behav. Biomed. Mater. 40 (2014) 178–189.
[14] M. Alvarez-Lopez, M.D. Pereda, J.A. Valle, M. Fernandez-Lorenzo, M.C. Garcia-Alonso, O.A. Ruano, et al., Acta Biomater. 6 (2010) 1763–1771.
[15] M. Bobby Kannan, W. Dietzel, R. Zettler, J. Mater. Sci. Mater. Med. 22 (2011) 2397–2401.
[16] B. Ratna Sunil, A.A. Kumar, T.S. Sampath Kumar, U. Chakkingal, Mater. Sci. Eng. C Mater. Biol. Appl. 33 (2013) 1607–1615.
[17] G.R. Argade, S.K. Panigrahi, R.S. Mishra, Corros. Sci. 58 (2012) 145–151.
[18] G.R. Argade, K. Kandasamy, S.K. Panigrahi, R.S. Mishra, Corros. Sci. 58 (2012) 321–326.
[19] N.N. Aung, W. Zhou, Corros. Sci. 52 (2010) 589–594.
[20] H. Wang, Y. Estrin, H. Fu, G.L. Song, Z. Zúberová, Adv. Eng. Mater. 9 (2007) 967–972.
[21] C. Op't Hoog, N. Birbilis, Y. Estrin, Adv. Eng. Mater. 10 (6) (2008) 579–582.
[22] G.B. Hamu, D. Eliezer, L. Wagner, J. Alloys Compd. 468 (2009) 222–229.
[23] H.E. Fridrich, B.L. Mordike, Magnesium Technology, Springer, Germany, 2006.
[24] B. Homayun, A. Afshar, J. Alloys Compd. 607 (2014) 1–10.
[25] D. Song, A. Ma, J. Jiang, P. Lin, D. Yang, J. Fan, Corros. Sci. 52 (2010) 481–490.
[26] R.Z. Valiev, R.K. Islamgaliev, I.V. Alexandrov, Prog. Mater. Sci. 45 (2) (2000) 103–189.
[27] R.S. Mishra, Z.Y. Ma, Mater. Sci. Eng. R Rep. 50 (2005) 1–78.
[28] B. Ratna Sunil, T.S. Sampath Kumar, U. Chakkingal, Mater. Sci. Forum 710 (2012) 264–269.
[29] R. Xin, B. Li, L. Li, Q. Liu, Mater. Des. 32 (Issues 8–9) (2011) 4548–4552.
[30] R. Xin, Y. Luo, A. Zuo, J. Gao, Q. Liu, Mater. Lett. 72 (2012) 1–4.
[31] G.-L. Song, JOM (1989) 64 (6) (2012) 671–679.
[32] Z. Pu, G.-L. Song, S. Yang, J.C. Outeiro, O.W. Dillon Jr., D.A. Puleo, et al., Corros. Sci. 57 (2012) 192–201.
[33] ASTM Standard, NACE TM0169/G31-12a. Standard Practice for Laboratory Immersion Corrosion Testing of Metals, ASTM International, West Conshohocken, PA, 2012, doi:10.1520/G0031-12A.
[34] F. Mansfeld, Advances in Corrosion Science and Engineering, vol. 6, Plenum Press, New York, 1970.
[35] B. Ratna Sunil, T.S. Sampath Kumar, U. Chakkingal, N.V. Mukesh Doble, J. Mater. Sci. Mater. Med. 25 (2014) 975–988.
[36] W.J. Arbegast, in: Z. Jin, A. Beaudoin, T.A. Bieler, B. Radhakrishnan (Eds.), Hot Deformation of Aluminum Alloys III, TMS, Warrendale, PA, USA, 2003.
[37] C.G. Rhodes, M.W. Mahoney, W.H. Bingel, M. Calabrese, Scr. Mater. 48 (2003) 1451–1455.
[38] R.S. Misra, P.S. De, N. Kumar, Friction Stir Welding and Processing: Science and Engineering, Springer, UK, 2014.
[39] M. Liu, D. Qiu, M.-C. Zhao, Script. Mater. 58 (2008) 421–424.
[40] R. Xin, B. Li, L. Li, Q. Liu, Mater. Des. 32 (2011) 4548–4552.